J Appl Electrochem (2009) 39:1297–1303
DOI 10.1007/s10800-009-9799-0

ORIGINAL PAPER

Electrodeposition of Al, Mn, and Al–Mn Alloy on aluminum electrodes from molten salt ($AlCl_3$–NaCl–KCl)

M. Jafarian · A. Maleki · I. Danaee · F. Gobal · M. G. Mahjani

Received: 10 March 2008 / Accepted: 12 January 2009 / Published online: 30 January 2009

Abstract Electrochemical deposition of aluminum and manganese from basic and acidic molten $AlCl_3$–NaCl–KCl mixture on an aluminum electrode at 180 °C was studied by the methods of voltammetry, and potential and current transient. The deposition of aluminum was found to proceed via a nucleation/growth mechanism in basic melt, while the deposition of manganese was found to be diffusion controlled in basic melt. The diffusion coefficient of Mn^{2+} ions in basic melt, as derived by voltammetry was in agreement with the deductions of transient methods. Analysis of the chronoamperograms indicates that the deposition of manganese on Al was controlled by 3D diffusion controlled nucleation and growth. The processes are manifested as peaks on a decaying chronoamperogram. Non-linear fitting methods were applied to obtain the kinetic parameters from theoretical formulae proposed to describe this system. It is also found that under more cathodic potentials, the saturation number density of the manganese nuclei and also the efficiency of use of the available surface nucleation sites increased.

Keywords Electrocrystallization · Nucleation · Growth · Aluminum · Manganese

M. Jafarian (✉) · A. Maleki · I. Danaee · M. G. Mahjani
Department of Chemistry, K. N. Toosi University of Technology, P. O. Box 15875-4416, Tehran, Iran
e-mail: mjafarian@kntu.ac.ir

F. Gobal
Department of Chemistry, Sharif University of Technology, P. O. Box 11365-9516, Tehran, Iran

1 Introduction

The electrocrystallization of metal deposits on foreign substrates continues to attract a great deal of interest in modern electrochemistry due to its technological importance [1]. Nucleation kinetics and growth of the first metallic nuclei formed on a substrate are critical steps that determine the physicochemical properties of electrodeposits and are crucial in the understanding and control of the process. The first stage, the nucleation on the substrate surface, is in fact an important step in all metal deposition processes [2–7]. This early stage of electrochemical phase transformation is usually associated with a one, two, or three dimensional nucleation process and the analysis of transients by means of different theoretical formalisms allows us to identify the different growth type or different steps which control or determine the nucleation processes (incorporation of atoms to the nuclei or diffusion) [8–12]. The formation and growth of an electrodeposit involves complex nucleation processes and several models have been proposed to describe the cathodic deposition of metals especially when the substrate and the electrodeposit are the same [13, 14]. It has also been shown that in many cases the electrolysis is mass transfer controlled and experiments have been devised to determine the diffusion coefficients of electroactive species [15].

In view of their interesting acid–base properties chloroaluminate melts (alkali metal chloride–$AlCl_3$ mixtures) have received considerable attention by molten salt chemists and a number of reports on the electrochemical and spectroscopic studies of both organic and inorganic substances in these media have appeared [16].

$AlCl_3$–NaCl melts has been employed as electrolytes for electrodeposition of metals and in rechargeable batteries. During the charging of a rechargeable battery based on

aluminum anodes, Hjuler et al. [17, 18] found that both aluminum dendrites and spongy deposits can be formed under certain circumstances. As previously demonstrated [19], spongy deposits of aluminum may be prevented by the addition of $MnCl_2$ and co-deposition of Al and Mn.

Amorphous alloys have received widespread attention because of their promising chemical, electrical, corrosion resistance, and mechanical properties [20]. Stafford [21] has studied the co-deposition of Al–Mn in a acidic chloroaluminate molten salt at 150 °C where it is claimed that deposition of Mn occurs cathodic of the deposition of $Al_2Cl_7^-$ species on account of no peak appearance. The onset of co-deposition has been reported to be at −0.3 V/Al.

Little work has been reported on studies by voltammetry, chronopotentiometry, and chronoamperometry in $AlCl_3$–NaCl–KCl melts. In our earlier work electrocrystallization of aluminum onto graphite from a molten electrolyte containing $AlCl_3$–NaCl–KCl was studied by the method of current transient and impedance spectroscopy [22, 23]. In the early stage of the deposition and at low cathodic potentials, two dimensional (2D) nucleation and layer-by-layer growth with some overlapping followed the initial double layer charging. The processes manifested themselves as peaks on decaying chronoamperograms. In impedance spectroscopy investigations, a model based on random birth and deterministic growth of monolayers was proposed in which the edges were assumed to follow a propagation law. Parameters of impedance model in this system could be calculated from the fitting of experimental data to the Faradaic impedance function derived theoretically.

It is the purpose of this study to investigate the electrochemical deposition of Al and Mn on aluminum electrode from basic NaCl–KCl–$AlCl_3$ molten salt. This system can be of great significance from the technological point of view because of its low vapor pressure and its low melting point of 115 °C. The kinetic of nucleation and growth of Mn on aluminum electrode is also studied by current transient.

2 Experimental

Materials used in this work were analytical grade and of Merck origin. $AlCl_3$ was redistilled while NaCl and KCl were dried for 4 h at 400 °C prior to use. Fused electrolyte having the composition 66–20–14 wt% ($AlCl_3$–NaCl–KCl) with the addition of 0.3 wt% anhydrous $MnCl_2$ were employed. Handling of the materials and the procedures for preparation of the fused electrolyte were much the same as reported previously [22]. The experiments were carried out at 180 °C.

The experiment were carried out in a conventional three electrode cell with a hand polished aluminum rod of 0.50 cm^2 surface area forming the working electrode. Its potential was monitored against an aluminum (99.999% purity) reference electrode directly immersed in the melt [16]. A large graphite rod was used as counter electrode.

The electrochemical cell was powered by an E.G&G model 273A potentiostat/galvanostat run by a PC through M270 commercial software. Cyclic voltammetry (CV), chronopotentiometry (CP) and chronoamperometry (CA) were employed. The data were analyzed through Statistica Stat Soft software.

3 Result and discussion

A cyclic voltammogram obtained in the potential range 0.2 to −0.9 V/Al at 180 °C with the scan rate of 60 mV s^{-1} is presented in Fig. 1. During the scan in the cathodic direction, a significant crystallization overpotential is noticed before aluminum electrodeposition occurs. The electroactive entity, probably $AlCl_4^-$, starts to reduce at −0.73 V/Al. In the reverse scan the cross-over loop signifying nucleation/growth in the course of a cathodic scan [24] is accompanied by the anodic dissolution peak of Al at −0.3 V/Al. On reversing the scan direction, metal already deposited on the electrode surface continues to grow as a result of the $AlCl_4^- + 3e \leftrightarrow Al + 4Cl^-$ reaction remaining thermodynamically and kinetically favorable.

The current step method is also a useful means of detecting the presence of nucleation. Potential maxima at the beginning of the transition time can be attributed to the nucleation process [25]. Experimental Chronopotentiograms exhibit a characteristic maximum in the early stages of deposition as shown in Fig. 2. At the very beginning of the chronopotentiogram, the steep falling potential has

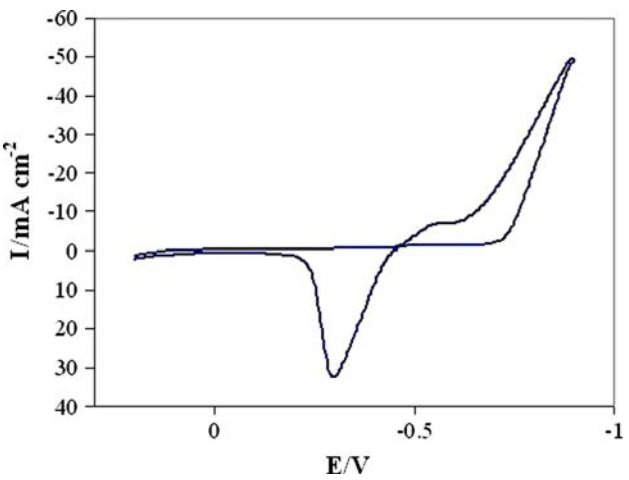

Fig. 1 Cyclic voltammogram of the aluminum electrode in basic molten salt (180 °C) without $MnCl_2$. The scan began at 0.2 V/Al with a scan rate of 60 mV s^{-1} and electrode area 0.5 cm^2

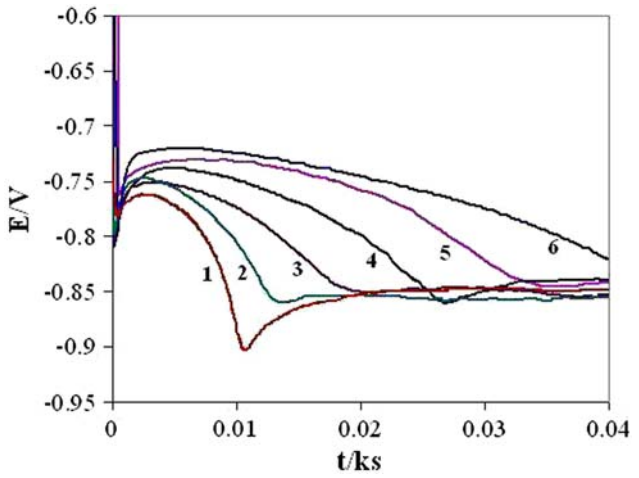

Fig. 2 Chronopotentiogram of the aluminum electrode in basic melt without $MnCl_2$ in different current density $I_1 = 16.5$, $I_2 = 15.95$, $I_3 = 15.55$, $I_4 = 15.1$, $I_5 = 14.6$, $I_6 = 14$ mA cm^{-2}

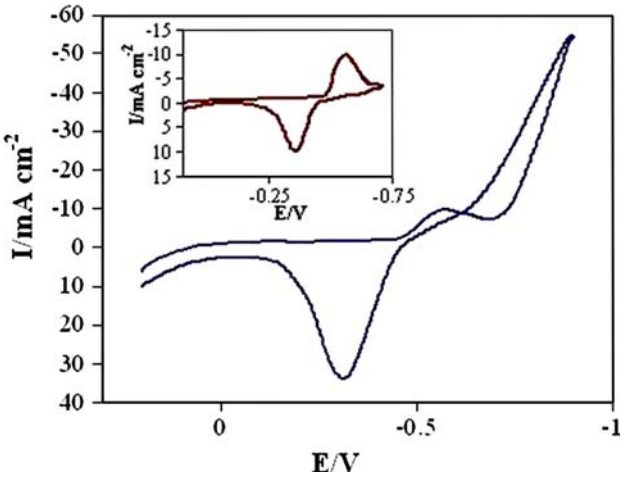

Fig. 3 Cyclic voltammogram of the aluminum electrode in basic melt in the presence of $MnCl_2$ (180 °C). The scan began at 0.2 V/Al with a scan rate of 60 mV s^{-1}. *Inset*: Cyclic voltammogram of the aluminum electrode in basic melt in limited potential range due to Mn deposition

contributions of both double layer as well as pseudo capacitor charging [26] due to adsorption followed by monolayer deposition of the electroactive constituents. As the potential increases, nucleation takes place [27] and an overvoltage is required to meet the galvanostatic conditions. As soon as nuclei start to grow, the overvoltage for reduction decreases. The product $I\tau^{1/2}$ was found to decrease with increasing current density, I, showing that the deposition of aluminum in basic melts is not controlled by diffusion and the reaction appears to be confined to the surface or near surface domains [28]. The decreasing trend suggests that a preceding chemical reaction mechanism similar to that observed in the $AlCl_3$–(Bupy)Cl electrolyte prevails [29].

A typical cyclic voltammogram at an aluminum electrode in a slightly basic melt (66–20–14 wt%) at 180 °C is shown in Fig. 3. The scan rate was 60 mV s^{-1} in the potential range 0.2 to −0.9 V/Al. The voltammogram obtained in the presence of $MnCl_2$ has the following features. In the cathodic scan the onset of the reduction peak at −0.46 V is clearly observed. A peak appears at −0.57 V, and is attributed to the reduction of Mn species. The peak current increases with scan rate and with $MnCl_2$ concentration. This peak is followed by the reduction of $AlCl_4^-$. This peak does not appear in the basic melt studies in the absence of manganese where only $AlCl_4^-$ is present. No overcrossing was observed in the direct and reverse scans and the dissolution peak of deposited manganese is observed at −0.35 V/Al. The ratio of the anodic peak current to the cathodic peak current obtained from Fig. 3 is nearly equal to one and also the coulombic charge associated with the deposition process is nearly equal to that of the stripping process. This indicates that the deposited manganese is an insoluble product with constant activity during the deposition and stripping process. A plot of peak current (I_p) versus the square root of scan rate (v) for the deposition processes exhibits a straight line which passes through the origin within experimental error (Fig. 4). This feature points to the diffusion controlled nature of manganese deposition in molten salts. From the slope of the straight line the diffusion coefficient of Mn^{2+} was obtained as $D_{Mn^{2+}} = 1.4 \times 10^{-6}$ cm^2 s^{-1}.

Chronopotentiometric measurements were also conducted with the aluminum electrode in slightly basic melt and in the presence of $MnCl_2$ and the results are shown in Fig. 5 where two steps appear in the chronopotentiograms.

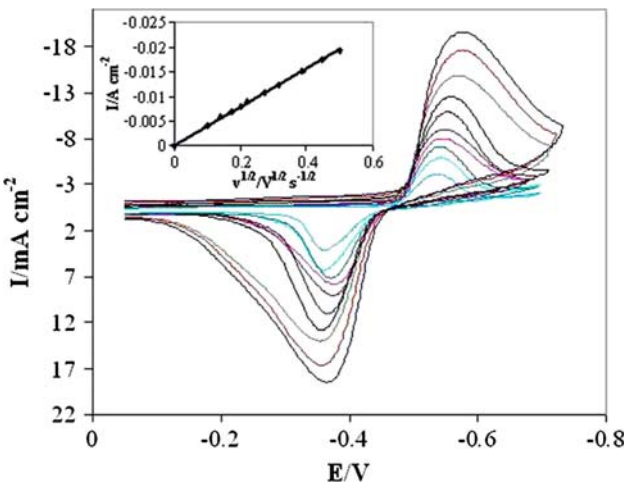

Fig. 4 Typical cyclic voltammograms of the aluminum electrode in basic melt in the presence of $MnCl_2$ (180 °C) in the potential sweep rates of 10, 20, 30, 40, 50, 75, 100, 150, 200, 250 mV s^{-1}. *Inset*: The proportionality of cathodic peak currents to the square roots of sweep rate

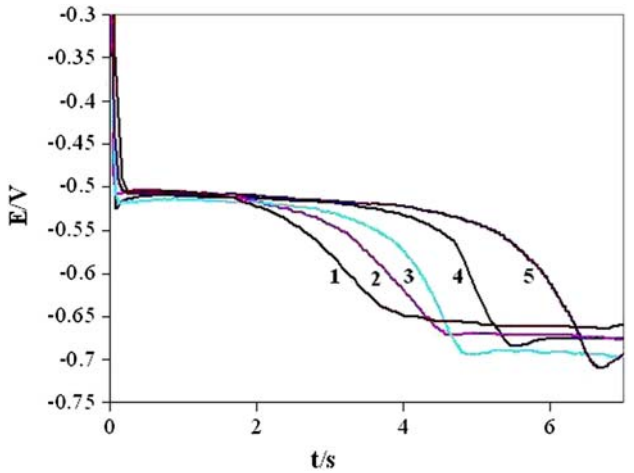

Fig. 5 Chronopotentiogram of the aluminum electrode in basic melt in the presence of $MnCl_2$ (180 °C) in different current density $I_1 = 6.4$, $I_2 = 5.9$, $I_3 = 5.4$, $I_4 = 4.8$, $I_5 = 4.2$ mA cm^{-2}

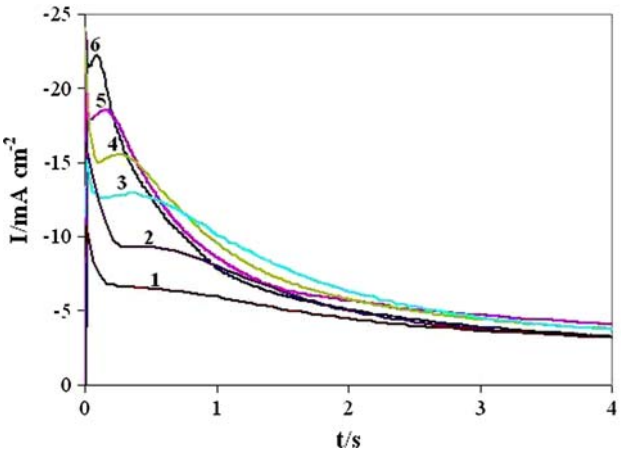

Fig. 6 Potentiostatic current transient obtained for deposition of Mn on aluminum at different potential: (1) −0.605, (2) − 0.61, (3) −0.615, (4) −0.62, (5) −0.625, (6) −0.63 V/Al

The first step is related to the reduction of ionic Mn species and is at a potential in agreement with that of the corresponding process in the cyclic voltammogram. The second step is related to $AlCl_4^-$ reduction in basic melt at −0.67 V at longer times. At the transition time, the potential rises sharply as the concentration of electroactive species at the electrode surface reaches zero. The product $I\tau^{I/2}$ was found to be constant with increasing current density, I, signifying that Mn^{2+} reduction is controlled by diffusion and Sand's law is obeyed. The diffusion coefficient derived from Sand's law is in very good agreement with that deducted from voltammetry and is found to be $D_{Mn^{2+}} = 2 \times 10^{-6}$ cm^2 s^{-1}. Logarithmic analysis of chronopotentiograms obtained in the diffusion controlled region gave good linear fits for the insoluble product model where the plot of E versus $\ln(\tau^{1/2} - t^{1/2})/\tau^{1/2}$ is linear and from its slopes the average value of n was calculated to be 2.4 in agreement with expectations from the equilibrium for reduction of Mn^{+2} (Eq. 1)

$$E = E_{th} + \frac{RT}{nF}\ln\left(\frac{\tau^{1/2} - t^{1/2}}{\tau^{1/2}}\right). \quad (1)$$

Figure 6 presents' chronoamperograms (CA) recorded at various applied cathodic potential steps in the range −0.6 and −0.63 V in the presence of $MnCl_2$. All transients are of the same shape with characteristic and well defined current maxima. In regard to the shape of the experimental current transients, the theory of Scharifker et al. [30] was used to account for a 3D nucleation and growth mechanism limited by diffusion of the electroactive species (3D-DC) and also to evaluate the kinetic parameters.

In the curves shown in Fig. 6 the fast decaying current corresponding to the charging of the double layer is followed by a rising current due to growth of the new phase and/or the increasing number of nuclei. At later stages the diffusion zones of adjacent nuclei overlap and the current density reaches a maximum followed by a decaying portion converging to a limiting current corresponding to the linear diffusion of the electroactive ions towards a planar electrode (Cottrell equation). The model of 3D-nucleation with hemispherical diffusion control of the growing 3D clusters accounts for the kinetics of electrolytic phase formation in the early stages when diffusion of the depositing species from the bulk of the solution to the electrode/solution interface is the slow step. Eventually overlap of diffusion zones and the development of nucleation exclusion zones around the already established nuclei prevail. The time necessary to reach current maximum (t_m) depends on the overpotential and decreases as the potential is made more cathodic.

As a preliminary step all current transients were presented in a non-dimensional form, a normalized current versus time [$(I/I_m)^2$ vs. t/t_m] plot. I_m and t_m correspond to the maximum current and time values used in the normalization processes [30]. According to this methodology a comparison of the theoretical plots with the experimental data allows the determination of nucleation process mechanism: instantaneous versus progressive.

The current–time dependencies of the two types are distinctly different and follow Eqs. 2 and 3.

$$\frac{I^2}{I_m^2} = 1.9542\left(\frac{t}{t_m}\right)^{-1}\left\{1 - \exp\left[-1.2564\left(\frac{t}{t_m}\right)\right]\right\}^2 \quad (2)$$

$$\frac{I^2}{I_m^2} = 1.2254\left(\frac{t}{t_m}\right)^{-1}\left\{1 - \exp\left[-2.3367\left(\frac{t}{t_m}\right)^2\right]\right\}^2 \quad (3)$$

for instantaneous and progressive processes, respectively.

Figure 7 shows such a non-dimensional plot for typical current transients recorded at different potentials for manganese deposition on aluminum. The relationship between

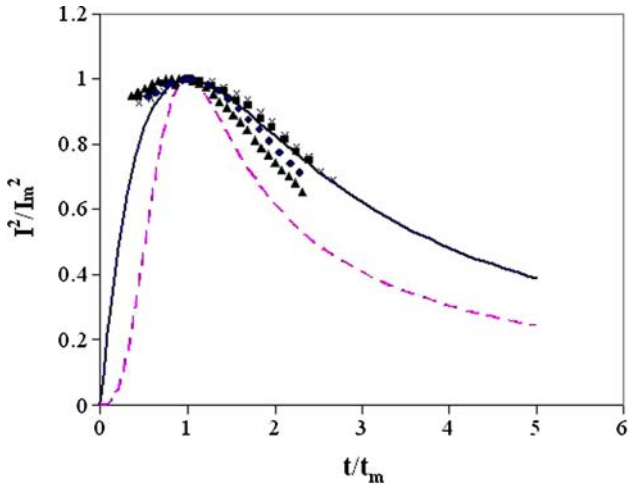

Fig. 7 Experimental and theoretical current transients compared and presented in a non-dimensional *I/Im* versus *t/tm*, plot, instantaneous (—) and progressive (- - -). Current transients associated with the peak, recorded at −0.615 (■) −0.62, (×) −0.625, (◆) −0.63 (▲) V/Al

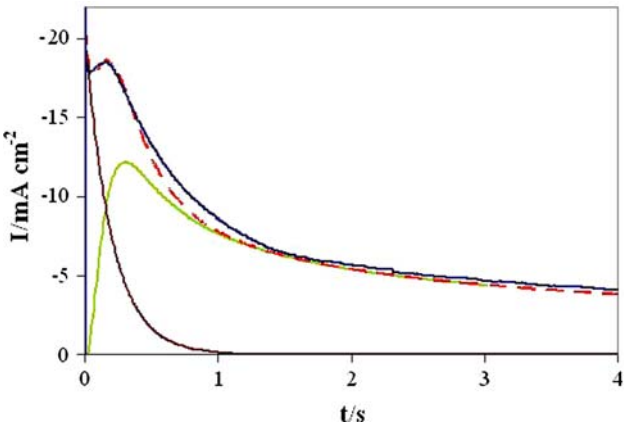

Fig. 8 Experimental current transient (—) recorded at −0.625 V and a corresponding theoretical curve (- - -) for 3D nucleation transition. Contributions to the transient current from the double layer charging phenomenon (I_{DL}) and 3D diffusion control nucleation processes (I_{3D}) are also shown

the experimental curves and the theoretical models remain the same at all potentials. These curves indicate an instantaneous type of nucleation. At overpotentials greater than −0.625 V, nucleation tends to switch toward the progressive type for $t > t_m$.

In the case when the nucleation mechanism changes with applied overpotential the evaluation of kinetic parameters based on the non-dimensional plots cannot be used. To estimate typical kinetic parameters for Mn deposition on to aluminum, we used Scharifker's [31] general equation (Eq. 4) for time evolution of the current density in the course of the 3D nucleation process limited by diffusion controlled growth ($I_{3D\text{-}DC}$).

$$I_{3D-DC} = \left(\frac{nFD^{1/2}C}{\pi^{1/2}t^{1/2}}\right) \times \left(1 - \exp\left\{-N_o\pi kD\left[t - \frac{1-\exp(-At)}{A}\right]\right\}\right). \quad (4)$$

This equation is equally valid for describing instantaneous and progressive nucleation and does not require distinction of the nucleation mechanism prior to its use. *nF* is the molar charge transferred during electrodeposition, *D* is the diffusion coefficient, and *C* is the bulk concentration of the electroactive species. Time is *t*, the number density of active sites is N_o, the nucleation rate constant is *A*, and Eq. 5 defines *k*.

$$k = \frac{4}{3}\left(\frac{8\pi CM}{\rho}\right)^{1/2} \quad (5)$$

M and ρ are the atomic weight and the density of the deposit, respectively.

The rate of nucleation does not remain constant during the electrocrystallization process, but decreases continuously due to the decline of the number density of active sites available for nucleation. Thus, the saturation number density of the formed manganese nuclei, N_s, is [30]

$$N_s = \left(\frac{AN_o}{2kD}\right)^{1/2}. \quad (6)$$

Taking into account the contribution of double layer charging in the current–time transient, $I_{DL} = k_1\, exp(-k_2 t)$, theoretical equations were fitted to the experimental current–transient (Fig. 8). The diffusion coefficient for ionic Mn species, characteristic kinetic parameters, the nucleation rate (*A*), number density of active sites (N_o), the AN_o product and the ratio N_s/N_o were obtained and are presented in Table 1.

As expected, in accordance with the theory, we found that *A*, N_o, and N_s increase with the application of more cathodic electrode potential. The N_s/N_o ratio, which can also be defined as the efficiency of the use of the available nucleation sites increase at more cathodic electrode potentials indicating that, at more negative potentials, higher surface sites are occupied by manganese nuclei.

The potential dependence of $\ln(N_s)$ is linear pointing to the exponential relationship between N_s and electrode potential. The potential dependence of N_o is due to distributed energies of nucleation on different sites. At low overpotentials, nucleation is restricted to very few active sites on the surface which become exhausted at an early stage in the process and nucleation thus approaches the instantaneous limit at low supersaturation. At very high cathodic overpotential the nucleation approaches progressive limit.

Table 1 Kinetic parameters obtained from the non-linear fitting of Eq. 4 with addition of double layer effect to the potentiostatic current transients shown in Fig. 5

E/V vs. Ag/AgCl	$D \times 10^6$/cm^2 s^{-1}	$N_o \times 10^{-7}$/cm^{-2}	A/s^{-1}	$AN_o \times 10^{-7}$/cm^{-2} s^{-1}	$N_s \times 10^{-7}$/cm^{-2}	N_s/N_o	$k_{1\ (DL)}$/A cm^{-2}	$k_{2\ (DL)}$/s^{-1}
−0.605	1.76	0.5	0.9	0.45	0.32	0.63	0.0025	2
−0.61	1.97	0.83	1.8	1.5	0.55	0.65	0.004	2.5
−0.615	2.2	1.08	2.8	3.03	0.74	0.68	0.0038	3
−0.62	2.2	1.15	5	5.76	1.02	0.88	0.005	4
−0.625	2.2	1.38	7	9.67	1.32	0.95	0.0052	5
−0.63	2.2	2.18	12	26.27	2.17	0.99	0.0056	7

Within the framework of the atomistic theory of nucleation [32], the number of atoms necessary to form the critical nucleus can be estimated directly from the potential dependence of the nucleation rate. The largest cluster for which the probability for attachment of one atom is less than one-half is defined as critical. The attachment of a new atom converts this cluster into a stable one for which the probability for attachment of the next atom is already higher than one-half and is henceforth able to grow spontaneously. According to the atomistic theory, the nucleation rate can then be expressed as

$$A = K_1 \exp\left(\frac{-W_k}{kT}\right) \exp\left(\frac{\alpha n e_o E}{kT}\right) \tag{7}$$

where K_1 is the pre-exponential factor, e_o the elementary electric charge, α is the cathodic transfer coefficient, E is the overpotential, and W_k is the reversible work for the formation of a critical nucleus consisting of N_k atoms. It has been shown [33] that, regardless of the nucleation model and for the case when the excess Gibbs energy of nucleus formation is potential dependent, N_k, A, E are related through

$$N_k = \frac{kT}{ne_o}\left(\frac{d\ln A}{dE}\right) - \alpha. \tag{8}$$

Equation (8) indicates that the slope of an experimental curve of ln$A$ versus E gives the size of the critical nucleus. The experimental ln$A$ versus potential plots for all concentrations studied in this work gave straight lines throughout the potential range. From their slope at 453 K and using a transfer coefficient value of 0.5, Eq. 8 the number of atoms that form critical nucleus was estimated to be 1.7 atoms.

4 Conclusion

Electrodeposition of aluminum and manganese onto an aluminum electrode from molten ($AlCl_3$–NaCl–KCl) salts was studied by the methods of cyclic voltammetry, chronopotentiometry, and chronoamperometry. Electrochemical deposition of aluminum onto aluminum electrode in basic melt was found to proceed via a nucleation/growth mechanism, while deposition of manganese from basic melts showed that ionic Mn species reduction was controlled by diffusion. The diffusion coefficient of this species (probably Mn^{2+}) was obtained by voltammetry, chronopotentiometry and is in agreement with the chronoamperometric measurements and was found to be 2×10^{-6} cm^2 s^{-1}.

Analysis of the chronoamperograms indicates that the deposition of manganese on Al substrates is 3D nucleation and growth controlled by diffusion. The magnitudes of the associated kinetic parameters and the parameter reflecting double layer charging in the initial stages of deposition have been reported. The kinetic parameters of the electrocrystallization of manganese increase with increasing applied potential. The efficiency of the use of the available nucleation sites at different potentials indicates that, at more cathodic potentials, a higher number of surface sites are occupied with manganese nuclei. On the basis of atomistic theory the number of atoms forming a critical nucleus was found to be 1.7.

References

1. Hjuler HA, Berg RW, Bjerrum NJ (1985) J Power Sources 10:1
2. Beratazzoli R, Pletcher D (1993) Electrochim Acta 38:671
3. Gomez E, Marin M, Sanz F, Valles E (1997) J Electroanal Chem 422:139
4. Cruz MS, Alanzo F, Palacois JM (1993) J Appl Electrochem 23:364
5. Trejo G, Ortega B, Meas VY, Ozil P, Chainet E, Nguyen B (1998) J Electrochem Soc 145:4090
6. Souteyrard E, Maruin G, Merciner D (1984) J Electroanal Chem 161:17
7. Gunawardena G, Hills G, Montenegro I, Scharifker B (1982) J Electrochem Soc 138:225
8. Astely DJ, Harrison JA, Thirsk HR (1968) Trans Faraday Soc 64:172
9. Fleischmann M, Thirsk HR (1960) Electrochim Acta 2:123
10. Gunawardena GA, Hills GJ, Montenegro I (1978) Electrochim Acta 23:693
11. Fleischmann M, Thirsk HR (1963) In: Delahay P (ed) Advanced electrochemistry and electrochemical engineering, vol 3. Academic Press, New York, p 123

12. Stranski IN, Kaishev R (1935) Z Physik 36:393
13. Volmer M (1921) Z Physik 22:646
14. Kaischew R, Mutaftschiew B (1965) Electrochim Acta 10:643
15. Kawamura K (1967) Electrochim Acta 12:1233
16. Jafarian M, Mahjani MG, Gobal F, Danaee I (2006) J Appl Electrochem 36:1169
17. Qingfeng L, Hjuler HA, Berg RW, Bjerrum NJ (1991) J Electrochem Soc 138:763
18. Rolland P, Mamantov GJ (1976) J Electrochem Soc 123:1299
19. Qingfeng L, Hjuler HA, Berg RW, Bjerrum NJ (1990) J Electrochem Soc 137:2794
20. Li JC, Nan SH, Jiang Q (1998) Surf Coat Technol 106:135
21. Stafford GR (1989) J Electrochem Soc 136:635
22. Jafarian M, Mahjani MG, Gobal F, Danaee I (2006) J Electroanal Chem 588:190
23. Jafarian M, Gobal F, Danaee I, Mahjani MG (2007) Electrochim Acta 52:5437
24. Greef R, Peat R, Peter LM, Pletcher D, Robinson J (1985) Instrumental methods in electrochemistry, Chap. 9. Ellis Horwood, Chichester
25. Hills DJ, Schriffrin DJ, Thomson J (1974) Electrochim Acta 19:657
26. Lantelme F, Chevalet J (1981) J Electroanal Chem 121:311
27. Gunawardena G, Hills G, Montenegro I, Scharifker B (1982) J Electroanal Chem 138:225
28. Stafford GR, Haarberg GM (1999) Plasma Ions 1:35
29. Qin QX, Skyllas-Kazacos M (1984) J Electroanal Chem 168:193
30. Scharifker BR, Hills G (1983) Electrochim Acta 7:879
31. Scharifker BR, Mostany J (1984) J Electroanal Chem 177:13
32. Milchev A, Stoyanov S, Kaichev R (1974) Thin Solid Films 22:267
33. Kaschiev D (1982) J Chem Phys 76:5098